Observation of a Velocity Domain Cooling Instability in a Radiative Shock

M. Hohenberger,[1,*] D. R. Symes,[2] J. Lazarus,[1] H. W. Doyle,[1] R. E. Carley,[1] A. S. Moore,[3] E. T. Gumbrell,[3] M. M. Notley,[2] R. J. Clarke,[2] M. Dunne,[2] and R. A. Smith[1]

[1]*Laser Consortium, Blackett Laboratory, Imperial College, London SW7 2BZ, United Kingdom*
[2]*Central Laser Facility, Rutherford Appleton Laboratory, Oxfordshire OX11 0QX, United Kingdom*
[3]*Plasma Physics Division, AWE Aldermaston, Reading RG7 4PR, United Kingdom*

(Received 29 January 2010; published 10 November 2010)

We report on experimental investigations into strong, laser-driven, radiative shocks in cluster media. Cylindrical shocks launched with several joules of deposited energy exhibit strong radiative effects including rapid deceleration, radiative preheat, and shell thinning. Using time-resolved propagation data from single-shot streaked Schlieren measurements, we have observed temporal modulations on the shock velocity, which we attribute to the thermal cooling instability, a process which is believed to occur in supernova remnants but until now has not been observed experimentally.

DOI: 10.1103/PhysRevLett.105.205003 PACS numbers: 52.35.Tc, 52.50.Jm, 52.72.+v

Shocks are a common phenomenon in both astrophysics and high-energy-density environments, and their understanding is vital for numerical models of complex plasma systems. If the energy deposition launching the shock is limited in time, it is followed by a rarefaction that catches up with the shock front and a blast wave is formed, often consisting of a thin shell containing much of the swept-up material [1]. A shock becomes *radiative* if the postshock conditions cause substantial cooling through radiative energy losses, resulting in fundamental structural and dynamical changes in the system evolution. Radiation is transmitted through the shock shell and, in an optically thin case, is lost from the system. In contrast, if the upstream material ahead of the shock front is sufficiently optically thick to parts of the emission spectrum, radiation is reabsorbed, leading to preheating and ionization of the upstream material. This can lead to growth of instabilities [2,3] which, in astrophysical scenarios such as the expansion of a supernova remnant, are believed to be of fundamental importance in seeding turbulence, resulting in the complex, knotted structures seen in high resolution telescope images.

The temporal expansion of a shock radius is often described as a power-law-type function of the form

$$R(t) \propto (E_0/\rho)^{\alpha/2} t^{\alpha}, \tag{1}$$

where E_0 denotes the deposited energy per unit length (in cylindrical geometry) and ρ is the ambient mass density. The term α is the deceleration parameter determined by the geometry and energy dissipation of the system, which for cylindrical, adiabatic blast waves is $\alpha = 0.5$ [4]. Equation (1) has been shown to be applicable to arbitrary energy loss rates ε where dissipative processes such as radiation or ionization remove energy from the shock [5]. The loss rate can be related to the pre- and postshock polytropic index, γ_1 and γ_2, respectively, via $\varepsilon = \frac{4(\gamma_1-\gamma_2)}{(\gamma_1-1)(\gamma_2+1)^2}$, such that energy losses ($\varepsilon > 0$) lead to a lowering of γ_2 compared to the unshocked value. Additionally, α is related to ε through Eqs. (2) and (4) in Ref. [5], and it can be shown that $\varepsilon > 0$ will result in a reduction of α to a value below the adiabatic solution; i.e., the blast wave decelerates more quickly. If radiative losses in the shell are sufficiently large that the shell cannot support itself any longer ($\varepsilon \approx 1$), it is pushed by the low-density but high-pressure interior of the shock and collapses to high densities. Specifically the transition to this *pressure-driven snowplow* regime and the associated shell thinning is thought to make the shock more susceptible to radiation-driven instabilities, one of which we address in this Letter.

Laser-driven radiative shocks have long been studied experimentally (e.g., [6–8]). One way to do so is by utilizing the efficient absorption of high-intensity lasers ($> 10^{14}$ W cm^{-2}) in clustered gases [9]. Using short-pulse lasers temporally decouples the initial energy deposition ($<$ ps) from the subsequent plasma evolution ($\geq$ ns), allowing one to study well-characterized shocked plasma systems under repeatable experimental conditions and with a varying degree of radiation [10–13]. Provided the geometry and key dimensionless parameters are matched to astrophysical phenomena, cluster targets can therefore be used to perform laser-driven shock experiments scalable to astrophysical systems [10,14].

The setup for the experiment presented in this Letter is described in detail in Ref. [15]. Clusters were generated by using a 500 μm orifice gas jet backed with cryogenically cooled H_2 at 42 bar or room temperature Ar or Kr at 52 and 35 bar, respectively [16]. The cluster gas was irradiated by using the Vulcan laser at the Rutherford Appleton Laboratory, with up to 60 J in a $\lambda = 1054$ nm, 1.4 ps FWHM pulse focused to 40 μm FWHM via an $f/18$ off-axis parabola. The focus was aligned into the cluster stream 3 mm above the center of the nozzle, generating cylindrical shocks over an energy deposition length of $h \approx 7.5$ mm. In a pump-probe geometry, the plasma evolution was backlit and imaged onto dark-field Schlieren and

Michelson interferometer setups using three separately timed $\lambda = 527$ nm, 1.3 ps probe beams providing spatially resolved snapshots of the interaction. These imaged the interaction onto CCD cameras from three angles orthogonal to the laser propagation direction. Additionally, each imaging setup distinguished between orthogonal polarizations, giving six separately timed snapshots for each laser shot [15]. The probe timing could be adjusted from 0 to 15 ns, while the polarization delay was variable from 0 to 3 ns. A calorimeter positioned after the interaction region measured transmitted laser energies (typically ~10%) while an array of infrared filtered diodes detected side-scattered radiation. As in similar experiments, no scatter was detected [9,17], giving absorption efficiencies of ~90%.

When determining the shock evolution from time-framed, multishot data, experimental fluctuations necessarily limit the accuracy of the extracted result. High resolution, early time-scale, single-shot propagation measurements have previously been demonstrated via spectrally resolving linearly chirped probe pulses [18]. In Ref. [19] long time-scale, single-shot measurements were demonstrated by using a long-duration optical backlighter to image the blast wave onto a streak camera via a Schlieren setup. By applying the latter method, the 6.8 ns pulse of a Q-switched, frequency doubled Nd:YAG laser (532 nm) was stretched to ~31 ns FWHM by passing it through a multireflection etalon array providing a smooth temporal profile. The elongated pulse was then used to image the plasma onto a streak camera via a Schlieren setup, recording the shock position with a temporal and spatial resolution of 50 ps and 20 μm, respectively.

Figure 1 shows typical shock front trajectories propagating away from the nozzle in H_2, Ar, and Kr and launched with 5, 6, and 11 J of deposited energy, while the inset shows the Kr Schlieren streak data. Superimposed onto the trajectories (solid lines) are power-law fits (dashed lines) used to extract time-averaged deceleration parameters. For clarity, error bars are shown only for H_2. From Eq. (1), the shock evolution is expected to depend on the parameter (E_0/ρ). This should therefore be kept constant in different target gases to allow a direct comparison of the trajectories for identification of potential energy loss mechanisms [12]. In Ar and Kr, this is the case with $2.3 \pm 0.6 \times 10^4$ and $2.9 \pm 0.5 \times 10^4$ J cm^2/g, respectively. However, limitations on the available gas pressure resulted in the energy density for H_2 exceeding that of the other gases by a factor of ~6. Since H_2 should not lose significant energy through radiation, it is therefore expected to expand much faster than the other two cases, as is observed in the data. Interestingly, the extracted deceleration parameter for H_2 exceeds 0.5 and therefore the prediction of the adiabatic solution. A contributing factor is the shock front propagating away from the nozzle and therefore down a density gradient. Furthermore, this could indicate a departure of the shock geometry from a purely cylindrical scenario. In any case, for gases of higher atomic number, the shock deceleration should be increasingly dominated by energy losses through radiation. Indeed, the shock trajectories for Ar and Kr for $t > 15$ ns both exhibit an $\alpha < 0.5$, suggesting that the blast waves are radiative during that time.

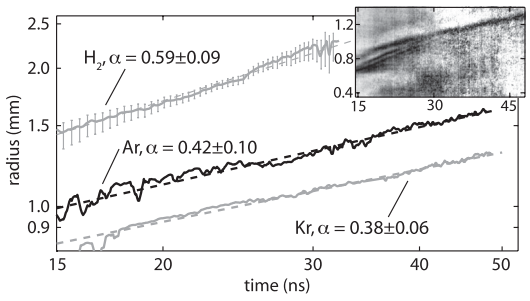

FIG. 1. Streaked Schlieren trajectory results in H_2, Ar, and Kr. For clarity, error bars are shown only for H_2. As expected, H_2 expands the fastest, while the deceleration parameter decreases with increasing atomic number. The inset shows the Kr streaked Schlieren data used to extract the trajectory.

This observation is consistent with radial electron density profiles of shocks extracted from short-pulse interferometry data via Abel inversion. The early time evolution of a shock launched in Ar with 6 J ($1.3 \pm 0.4 \times 10^4$ J cm^2/g) is displayed in Fig. 2. At 6 ns (gray line) the shock, propagating from left to right, has reached 600 μm and is already well resolved. Ahead of the shock front an ionization precursor indicative of energy transport is visible. At 12 ns (black line) the shock is significantly more pronounced with the shell thickness Δr having decreased by 60%. Additionally, the upstream gas is heated further, resulting in a doubling of the electron density, while the postshock density is reduced. From an estimated preheat temperature of a few eV, the electron mean free path is not expected to exceed 20 μm, such that the extent of the ionization precursor (> 400 μm) provides evidence of the strongly radiative nature of these shocks. By using the observed shell thickness, the compression, i.e., the shocked mass density divided by the ambient density, can be estimated to be as high as $C \approx 5.5$ for the late-time snapshot. While higher compression can be achieved in high-energy, piston-driven shocks [7], this is the highest

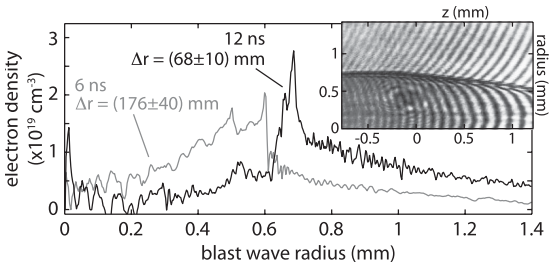

FIG. 2. An Ar shock launched with 6 J exhibits a strong radiative precursor and significant reduction of the shell thickness Δr. Both profiles were obtained on the same shot. The inset shows the original 12 ns interferometric data.

compression so far reported in shocks in *clustered* media. In contrast to previous measurements in clusters at lower drive energies [12,13], this exceeds the ideal gas compression limit ($C = 4$), further underlining the importance of dissipative processes in shocks under these experimental conditions even in a moderate Z target gas such as Ar.

Interestingly, assuming an equal ionization rate, the shocked mass in the 12 ns image seems less than would be expected from a simple geometric account of the swept-up mass between the two displayed times. However, this is explained by noting that the peak electron densities generated at the shock front result in very strong and hard-to-resolve fringe shifts in the interferometric data (see the inset in Fig. 2). Specifically, in the 12 ns data, the fringes are difficult to trace around the peak and the displayed data should be considered a minimum value. It is conceivable that the peak fringe shift is, in fact, underestimated by a factor of 2π, equivalent to one full fringe shift. This would raise the peak value to $\sim 3.5 \times 10^{19}$ cm^{-3}, thus solving the mass discrepancy.

Shell thinning is an important feature in radiative blast waves as it is expected to make a shock more susceptible to instabilities such as the dynamic spatial overstability [3] or the thermal cooling instability (TCI) [2]. While a considerable body of experimental work has been devoted to the former [6,11], the latter has received only limited experimental attention and, thus far, could not be verified experimentally [19]. Through numerical investigations, this instability is thought to be responsible for a deviation of the ultraviolet and optical emission spectra away from those expected for steady-state flow conditions, for example, in the Cygnus loop or the Vela supernova remnant [2]. The TCI occurs when a shock begins to stall by losing kinetic energy through radiation but then reforms as it expands into the radiatively preheated medium. As a result, this instability is expected to cause a temporal oscillation of the shock velocity, as the shock front periodically loses and gains energy. The onset of the TCI is determined by the radiative cooling function of a gas with electron temperature T_e, given locally by $\Lambda(T_e) \propto T_e^{\beta}$. A shock is expected to be susceptible to the TCI if β fulfills the condition $\beta = d(\log\Lambda)/d(\log T_e) \leq 1$ [20]. For astrophysical shocks, a velocity threshold of $u_s \geq 120$ km s^{-1} has been calculated for the TCI to occur [21]. However, since it depends only on the shape of the cooling function with temperature, it is conceivable to study the TCI on a laboratory scale at lower temperature and shock velocity provided the condition for β is satisfied.

Earlier experimental studies identified Kr as the most likely candidate to undergo the TCI under the experimental conditions accessible in laser-driven shocks in cluster media, with no significant radiative cooling in H_2 and cooling in Ar scaling with $\beta > 2.5$ [19]. While this could not be demonstrated at the 1 J drive level, it was deemed possible that faster and hotter shocks can potentially enter a regime susceptible to the TCI. Results for the shock velocity evolution in Kr launched with roughly 1-order-of-magnitude higher energies can be seen in Fig. 3. It was obtained by averaging the shock propagation from a streaked Schlieren measurement in 2 ns intervals, chosen such that the shock expansion during this time step exceeds the spatial resolution. In Fig. 3(a), the shock was launched with a deposited energy of 8 J ($2.1 \pm 0.5 \times 10^4$ J cm^2/g), and, for $t > 15$ ns, the velocity very closely follows an averaged deceleration with $\alpha = 0.38$ (dashed line), the deceleration predicted for a fully radiative shock disregarding ionization [5]. While variations in the shock velocity are visible, they are too small to be interpreted as characteristic oscillations. In stark contrast, Fig. 3(b) shows the shock velocity evolution of a blast wave in Kr launched with higher energy (11 J) and $2.9 \pm 0.5 \times 10^4$ J cm^2/g. The averaged data (dashed line) again yield $\alpha = 0.38$, but the time-resolved velocity now undergoes strong, well-resolved oscillations in time with a period of $\Delta t \sim$ 7–9 ns and an amplitude as high as $\sim$50% of the maximum velocity. Note that the data in Fig. 3(b) are the same as used in Fig. 1.

An estimate of the oscillation time based on the TCI mechanism can be made by calculating the time it takes for the shock to radiate away all of its kinetic energy. Through knowledge of the shock speed, the total kinetic energy in the shock in Fig. 3(b) is $\approx$ 2.4 J. While the cooling rate at laboratory conditions is unknown, Keilty *et al.* have compared astrophysical values to numerically calculated ones and find close agreement in Kr [5]. Using the data published in Ref. [22], the radiative cooling coefficient at the density of the compressed gas in the shock shell ($\sim 10^{19}$ cm^{-3}) can be extrapolated to be $\sim 4.6 \times 10^{-34}$ W m^3, which results in an estimated energy loss rate of $\sim 4 \times 10^8$ J/s and a cooling time of $\sim$6 ns. Given that cooling function data are available only for astrophysical densities, this is at best an order-of-magnitude estimate. Yet, it agrees surprisingly well with the oscillation

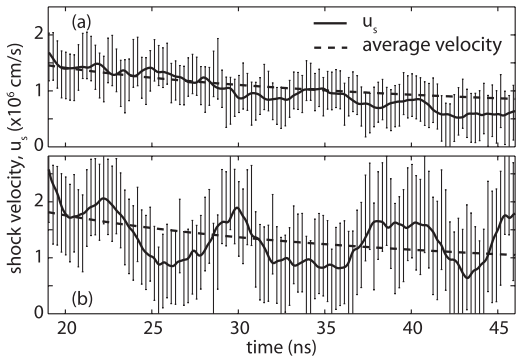

FIG. 3. Temporal expansion velocity evolution of blast waves in Kr. Both shocks launched with (a) 7 and (b) 11 J decelerate with an averaged $\alpha = 0.38$. While (a) shows no unambiguous modulation, (b) exhibits significant oscillations in the shock velocity believed to be caused by the TCI.

period of $\Delta t \sim 7$–9 ns visible in the shock velocity in Fig. 3(b).

Following the discussion in Ref. [5], it is also possible to estimate the energy loss directly. To this end we use a generalized energy equation which has to be equal on both sides of the shock front [23], i.e., $E_1 = E_2$, with

$$E = \rho u\left[\frac{u^2}{2} + \frac{\gamma}{\gamma - 1}\frac{k_B T}{m_A}(1 + \langle Z\rangle) + E_e\right] + \frac{4}{3}uaT^4. \quad (2)$$

Here, ρ, m_A, u, γ, and T are the mass density, atomic mass, fluid velocity in the shock frame, polytropic index, and temperature, respectively. $\langle Z\rangle$ and E_e denote the effective ionization of the gas and the associated excitation energy, respectively. The values k_B and a are the Boltzmann and radiation constant, respectively.

In the precursor, the shock velocity u_1 as well as the ionization $\langle Z_1\rangle$ is extracted directly from the data, while ρ_1 is obtained from gas jet characterization measurements. Through $\langle Z_1\rangle$, one can estimate the precursor E_e via known ionization potentials [24]. Assuming local thermal equilibrium and following an extrapolation method detailed in Ref. [4], an average ionization of $\langle Z_1\rangle = 2.9$ gives $T_1 = 4.8$ eV. Regarding the postshock values, the gas velocity as well as the density is obtained experimentally through measurement of the compression C and substituting $\rho_2 = C\rho_1$ and $u_2 = u_1/C$. This also gives the effective ionization and, by using the same arguments as above, translates to an effective temperature ($\langle Z_2\rangle = 3.3$, $T_2 = 6.3$ eV), leaving only the pre- and postshock polytropic indices unknown. Naturally, upon choosing the preshock value γ_1, the postshock γ_2 is determined through the requirement for energy balance, i.e., Eq. (2). We estimate $\gamma_1 = 1.2$ [1] and find $\gamma_2 = 1.1$. Using these results we calculate the energy dissipation ε as defined in the introduction and finally the energy loss rate via $dE/dt = -\pi R h \rho_1 u_1^3 \varepsilon$ [5]. This equates to 3.5×10^8 J/s, which agrees well with the cooling rate extrapolated from astrophysical values and again confirming an expected oscillation rate on the order of a few nanoseconds, as is observed in the experimental data.

The observation of shock velocity oscillations is extremely promising and elegantly demonstrates the capability of the streaked Schlieren technique to observe the TCI. In conjunction with the very good agreement between the estimated cooling time and the experimental result, we deduce that this is the first experimental observation of the TCI. While the discussed experiment was not designed as a scaled astrophysical scenario, the demonstration that this numerically predicted instability can be generated in a lab-scale environment is an important step towards properly scaled experiments with full astrophysical relevance.

In conclusion, we have presented data from recent experimental investigations of laser-driven shocks in cluster media. The shocks were driven with significantly higher energy densities than in previous experiments, and the data clearly show stronger radiative effects than previously observed in shocked cluster media. This includes a decreased deceleration parameter, shell thinning, and enhanced compression exceeding the theoretical strong shock limit for an ideal gas. Furthermore, the temporal evolution of shocks in Kr was investigated by means of the single-shot streaked Schlieren technique. The shock velocity data show strong oscillations as a function of time, which we believe constitutes the first experimental observation of the thermal cooling instability.

We are pleased to acknowledge useful discussions with R. P. Drake and are grateful for the technical assistance by P. Ruthven, A. Gregory, and B. Ratnasekara as well as the Central Laser Facility technical staff and laser operators. This work was supported by EPSRC and MoD UK.

*M.Hohenberger04@Imperial.ac.uk

[1] R. P. Drake, *High-Energy-Density Physics: Fundamentals, Inertial Fusion, and Experimental Astrophysics* (Springer, New York, 2006).
[2] R. A. Chevalier and J. N. Imamura, Astrophys. J. **261**, 543 (1982).
[3] E. T. Vishniac, Astrophys. J. **274**, 152 (1983).
[4] Y. B. Zel'Dovich and Y. P. Raizer, *Physics of Shock Waves and High-Temperature Hydrodynamic Phenomena* (Academic, New York, 1966).
[5] K. A. Keilty *et al.*, Astrophys. J. **538**, 645 (2000).
[6] J. Grun *et al.*, Phys. Rev. Lett. **66**, 2738 (1991); A. D. Edens *et al.*, Phys. Rev. Lett. **95**, 244503 (2005).
[7] S. Bouquet *et al.*, Phys. Rev. Lett. **92**, 225001 (2004); A. B. Reighard *et al.*, Phys. Plasmas **13**, 082901 (2006).
[8] M. Koenig *et al.*, Phys. Plasmas **13**, 056504 (2006); P. A. Keiter *et al.*, Phys. Rev. Lett. **89**, 165003 (2002).
[9] T. Ditmire *et al.*, Phys. Rev. Lett. **78**, 3121 (1997).
[10] K. Shigemori *et al.*, Astrophys. J. **533**, L159 (2000).
[11] M. J. Edwards *et al.*, Phys. Rev. Lett. **87**, 085004 (2001).
[12] A. S. Moore *et al.*, Astrophys. Space Sci. **307**, 139 (2007).
[13] J. Osterhoff *et al.*, New J. Phys. **11**, 023022 (2009).
[14] D. Ryutov *et al.*, Astrophys. J. **518**, 821 (1999); Phys. Plasmas **8**, 1804 (2001); D. R. Symes *et al.*, High Energy Density Phys. **6**, 274 (2010).
[15] M. Hohenberger *et al.*, CLF Annual Report 2007–2008, 2008 (unpublished), p. 23.
[16] R. A. Smith, T. Ditmire, and J. W. G. Tisch, Rev. Sci. Instrum. **69**, 3798 (1998).
[17] E. T. Gumbrell *et al.*, New J. Phys. **10**, 123011 (2008).
[18] A. Benuzzi-Mounaix *et al.*, Phys. Rev. E **60**, R2488 (1999); D. Batani *et al.*, Phys. Plasmas **16**, 033104 (2009).
[19] A. S. Moore *et al.*, Phys. Rev. Lett. **100**, 055001 (2008).
[20] R. S. Sutherland, G. V. Bicknell, and M. A. Dopita, Astrophys. J. **591**, 238 (2003).
[21] P. A. Kimoto and D. F. Chernoff, Astrophys. J. **485**, 274 (1997).
[22] K. B. Fournier *et al.*, Nucl. Fusion **40**, 847 (2000).
[23] C. Michaut *et al.*, Eur. Phys. J. D **28**, 381 (2004).
[24] E. B. Saloman, J. Phys. Chem. Ref. Data **36**, 215 (2007).